J Bionic Eng 15 (2018) 636–646
DOI: https://doi.org/10.1007/s42235-018-0052-6

Journal of Bionic Engineering
http://www.springer.com/journal/42235

Aerodynamic Performance of a Flapping Foil with Asymmetric Heaving Motion near a Wall

Xingjian Lin[1], Shuhao Guo[1], Jie Wu[1,2*], Jingwen Nan[1]

1. *Department of Aerodynamics*, *Nanjing University of Aeronautics and Astronautics*, *Nanjing* 210016, *China*
2. *State Key Laboratory of Mechanics and Control of Mechanical Structures*, *Nanjing University of Aeronautics and Astronautics*, *Nanjing* 210016, *China*

Abstract

The effect of asymmetric heaving motion on the aerodynamic performance of a two-dimensional flapping foil near a wall is studied numerically. The foil executes the heaving and pitching motion simultaneously. When the heaving motion is symmetric, the mean thrust coefficient monotonically increases with the decrease in mean distance between foil and wall. Meanwhile, the mean lift coefficient first increases and then decreases sharply. In addition, the negative mean lift coefficient appears when the foil is very close to the wall. After the introduction of asymmetric heaving motion, the influence of wall effect on the force behavior becomes complicated. The mean thrust coefficient is enhanced when the duration of upstroke is reduced. Moreover, more and more enhancement can be achieved when the foil approaches the wall gradually. On the other hand, the positive mean lift coefficient can be observed when the duration of downstroke is shortened. By checking the flow patterns around the foil, it is shown that the interaction between the vortex shed from the foil and the wall can greatly modify the pressure distribution along the foil surface. The results obtained here might be utilized to optimize the kinematics of the Micro Aerial Vehicles (MAVs) flying near a solid wall.

Keywords: asymmetric heaving motion, wall effect, thrust enhancement, positive mean lift

1 Introduction

The wall effect can be frequently observed in the propulsion of flyers and swimmers in nature. It can lead to the drag reduction or lift enhancement, which is the most appealing dynamic advantage for the flyers and swimmers[1,2]. For example, the black skimmer is found to achieve high lift-to-drag ratio when flying above the water surface[3,4], the pelican can save energy consumption when gliding near the water surface[5], the steelhead trout can experience a high propulsion efficiency when swimming near the channel wall[6], and the similar dynamic advantage can be found in many other flyers and swimmers when advancing near the wall[7,8].

The wall effect was first investigated by fixing a wing near the wall in a wind tunnel, which is called as steady wall effect[1]. It was found that the lift-to-drag ratio could be as high as 20 or more if the clearance between the foil and the wall is less than a threshold value[9]. Such high lift-to-drag ratio is the consequence of increased lift due to the high underside pressure and low induced drag due to reduced wing-tip vortices[10]. Besides the clearance between the wing and the wall, the flow characteristics, such as the viscosity, inlet velocity, and the Reynolds number and so on, are also found to influence the wall effect[11,12]. Moreover, Rayner[13] pointed out that the higher aspect ratio of wing could achieve more dynamic advantage from the wall effect. The steady wall effect has been extensively studied so far, and there are many successful applications, such as the air cushion vehicles, the wing-in-wall-effect craft, and the racing car[2].

On the other hand, when the animals move forward near the wall, the clearance between the wings (or fins) and the wall changes periodically, which then is called as unsteady wall effect[1]. Compared with the steady wall effect, the unsteady wall effect is more complex due to the changing clearance, which would induce the complex vortex-structure interactions. Thus, in recent years, the unsteady wall effect has been studied extensively.

Srinidhi and Vengadesan[14] indicated that the presence of the wall would cause the vortices rebound.

***Corresponding author:** Jie Wu
E-mail: wuj@nuaa.edu.cn

As a result, the effective angle of attack of the flapping foil would change, and then the force generation is influenced. Dai *et al.*[15] stated that the secondary vortex generated by the wall would affect the vortex pairing and rebounding. Fernández-Prats *et al.*[16] showed that the introduction of the wall could enhance the momentum distribution along the propulsive direction. Gao and Lu[17] found that there were three regimes of lift behavior, *i.e.*, enhancement, reduction, and recovery regime, as the clearance increased.

In addition, Kolomenskiy *et al.*[18] numerically investigated the unsteady wing-wake interactions. They pointed out that the steady wing kinematics was beneficial for achieving the positive wall effect. Wu *et al.*[19] indicated that the flapping frequency of foil could influence the unsteady wall effect. They found that the presence of the wall would reduce the drag at the high frequency. Truong *et al.*[20,21] experimentally investigated the wall effect during the takeoff of beetle. They demonstrated that the unsteady wall effect that enhanced the lift was mainly working during the downstroke but negligible during the upstroke.

As seen from the previous studies, it is known that both the clearance and the wing kinematics influence the unsteady wall effect greatly. However, the further understanding of the unsteady wall effect is still required. For example, there is very little study about the unsteady wall effect of a wing with asymmetric motion. Therefore, the unsteady wall effect of a two-dimensional foil, which simultaneously executes the asymmetric heaving motion and the traditional pitching motion near a wall, is investigated numerically in this work. Based on the numerical results obtained, the influence of asymmetric motion with wall effect on the force behavior of the flapping foil is analytically displayed.

2 Problem definition and methodology

2.1 Problem definition

In the current study, a two-dimensional NACA0012 airfoil is used to represent the model of wing, as shown in Fig. 1a. The freestream velocity is U_0, and the chord length of foil is c. The foil, which simultaneously performs the heaving and pitching motion, is placed near a solid wall. The heaving motion is asymmetric, and the pitching motion is traditional. So the flapping motion is

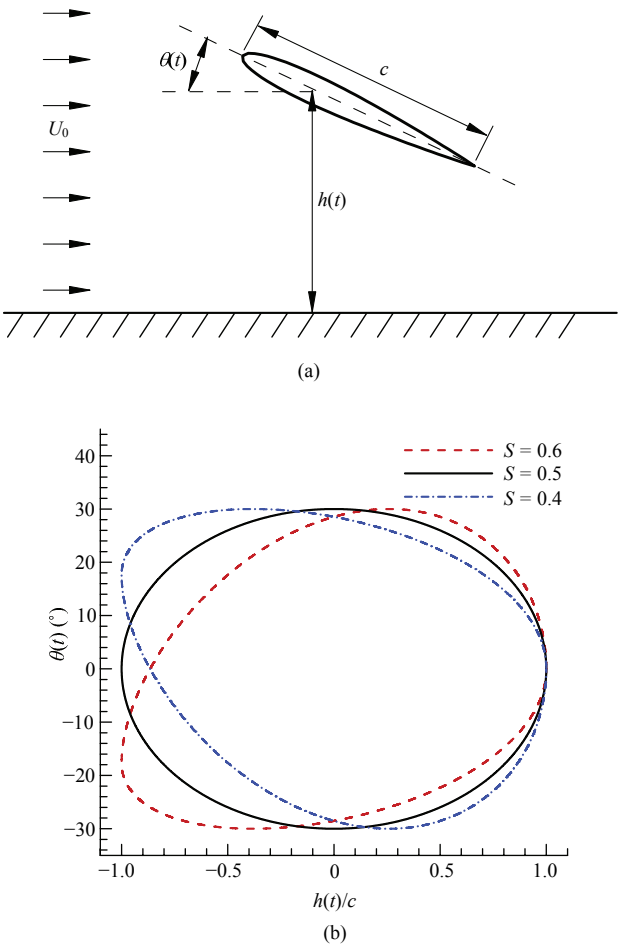

Fig. 1 (a) Sketch of a flapping foil near a solid wall and (b) $h(t)$–$\theta(t)$ phase diagram.

prescribed as[22]:

$$\theta(t) = \theta_0 + \theta_m \sin(2\pi f t), \tag{1}$$

$$h(t) = \begin{cases} h_0 + h_m \cos\left(2\pi\left(\dfrac{t^*}{2S}\right)\right), & 0 \le t^* \le S \\ h_0 + h_m \cos\left(2\pi\left(\dfrac{1-t^*}{2(1-S)}\right)\right), & S < t^* \le 1 \end{cases}, \tag{2}$$

where $\theta(t)$ is the instantaneous pitching angle, θ_0 is the mean angle of attack, θ_m is the pitching amplitude, $h(t)$ is the clearance between the foil and the wall, h_0 is the mean value of clearance, h_m is the heaving amplitude, f is the flapping frequency, t is the time, $t^* = ft - \mathrm{int}(ft) = \mathrm{mod}(t/T)$, T is the flapping period. S is the asymmetric coefficient, which describes the asymmetric level. For example, as shown in Fig. 1b, $S = 0.4$ means that the downstroke consumes 40% of one cycle time, whilst

S = 0.5 represents the symmetric heaving motion. In addition, the pitching axis is fixed at quarter-chord in this study.

2.2 Numerical method

In this study, the two-dimensional viscous flow over the flapping foil is governed by the Navier-Stokes equations[23]:

$$\frac{\partial \rho}{\partial t} + \nabla \cdot (\rho \boldsymbol{u}) = 0, \tag{3}$$

$$\frac{\partial \rho \boldsymbol{u}}{\partial t} + \nabla \cdot (\rho \boldsymbol{u}\boldsymbol{u} + p\boldsymbol{I}) = \mu \nabla \cdot \left[\nabla (\rho \boldsymbol{u}) + \nabla (\rho \boldsymbol{u})^{\mathrm{T}} \right], \tag{4}$$

where ρ is the flow density, $\boldsymbol{u}$ is the flow velocity vector, p is the pressure, μ is the dynamic viscosity of the flow, and $\boldsymbol{I}$ is the unit tensor. For the case of small density-variation and low Mach number, Eqs. (3) and (4) can be used to simulate incompressible flows[23]. By the finite volume method, they can be discretized as[24]:

$$\frac{\mathrm{d}\boldsymbol{W}_J}{\mathrm{d}t} = -\frac{1}{\Omega_J} \sum_{i=1}^{N_f} \boldsymbol{F}_{ni} S_i, \tag{5}$$

$$\boldsymbol{W} = (\rho, \rho u, \rho v)^{\mathrm{T}} ?, \tag{6}$$

$$\boldsymbol{F}_n = (F_\rho, F_{\rho u}, F_{\rho v})^{\mathrm{T}}, \tag{7}$$

where $\boldsymbol{W}$ is the conservative variable vector, $\boldsymbol{F}_n$ is the numerical flux vector, J is the index of the control cell, Ω_J denotes the volume of the control cell J, N_f represents the number of the face of the control cell J, and S_i is the area of the ith interface of the control cell J, u and v represent the horizontal and vertical velocities in the global Cartesian coordinate system defined at the cell center, respectively.

Eq. (5) is a flux equation, and the key to solve this equation is to calculate numerical fluxes $\boldsymbol{F}_n$. As a consequence, the local coordinate system defined at the cell interface is introduced[23]:

$$\boldsymbol{W} = \boldsymbol{n} \cdot \bar{\boldsymbol{W}}, \tag{8}$$

$$\boldsymbol{F}_n = \boldsymbol{n} \cdot \bar{\boldsymbol{F}}_n, \tag{9}$$

where $\boldsymbol{n}$ denotes the unit vector of the local coordinate system, $\bar{\boldsymbol{W}}$ and $\bar{\boldsymbol{F}}_n$ represent the conservative variables and the numerical fluxes in the local coordinate system, respectively, which can be expressed as[23]:

$$\bar{\boldsymbol{W}} = (\rho, \rho u_1, \rho u_2)^{\mathrm{T}}, \tag{10}$$

$$\bar{\boldsymbol{F}}_n = (F_\rho, F_{\rho u_1}, F_{\rho u_2})^{T}, \tag{11}$$

where $\boldsymbol{u} = (u_1, u_2)$ is the velocity vector in the local coordinate system.

In this work, a simplified circular function-based gas kinetic scheme[23] is used to calculate the fluxes in the local coordinate system, which is written as[23]:

$$\bar{\boldsymbol{F}}_n = \boldsymbol{F}^I + \tau_v^* \left[\boldsymbol{F}^{\mathrm{II}} - \boldsymbol{F}^{\mathrm{I}} \right], \tag{12}$$

where $\tau_v^* = \tau_v / \delta t$, δt is the streaming time which is calculated as δt = 0.4min(Δl,Δr)/(max(u_1^+,u_2^+)+c_s), where $c_s = \sqrt{2} U_0 / Ma$, Δl and Δr represent the lengths of the shortest edges of the left and right cells around the interface, respectively. The details of F^{II} and F^{I} can be found in Ref. [23].

In order to simulate the fluid-structure interactions between the flapping foil and the surrounding flow, a velocity correction-based immersed boundary method[25] is employed. In this method, the flow velocity is implicitly corrected by the no-slip boundary condition. For more details, one can refer to our previous work[19,25].

2.3 Numerical validation

To validate the adopted numerical method, the simulation of a flapping foil near a wall is carried out. The parameters used are the same as our previous work[19]. The size of computational domain is $25c \times 25c$. A non-uniform mesh is used, which is fine and uniform around the foil, and the spacing of uniform mesh is $\Delta h = 0.025c$. The Reynolds number, $Re = \rho U_0 c/\mu$, is 150, and other parameters are h_0/c = 3, h_m/c = 0.4, θ_0 = 0, $\theta_m = \pi/4$ and f = 0.125. Fig. 2 shows the time histories of drag coefficient (C_{D}) and lift coefficient (C_{l}) of the foil. It can be seen from the figure that the current result agrees well with that of Wu *et al.*[19]. Therefore, the adopted method is suitable for the current investigation.

3 Results and discussion

In this section, the aerodynamic performance of a rigid flapping foil with asymmetric heaving motion in wall effect is studied in detail. It should be pointed out that, in order to simplify the problem, the effect of the foil deformation is not considered in this work, although the flexibility and deformation also influence

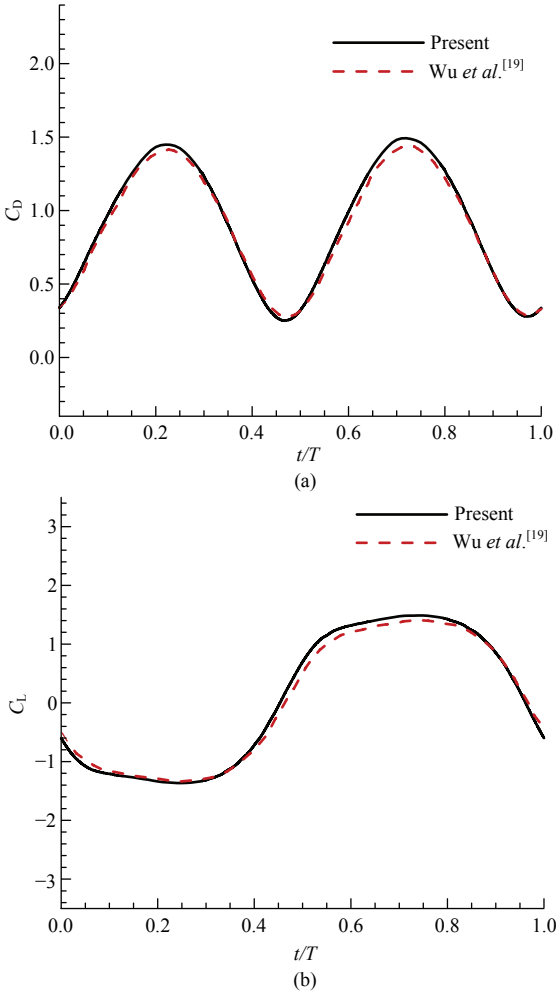

Fig. 2 Time histories of (a) drag coefficient and (b) lift coefficient obtained from different methods.

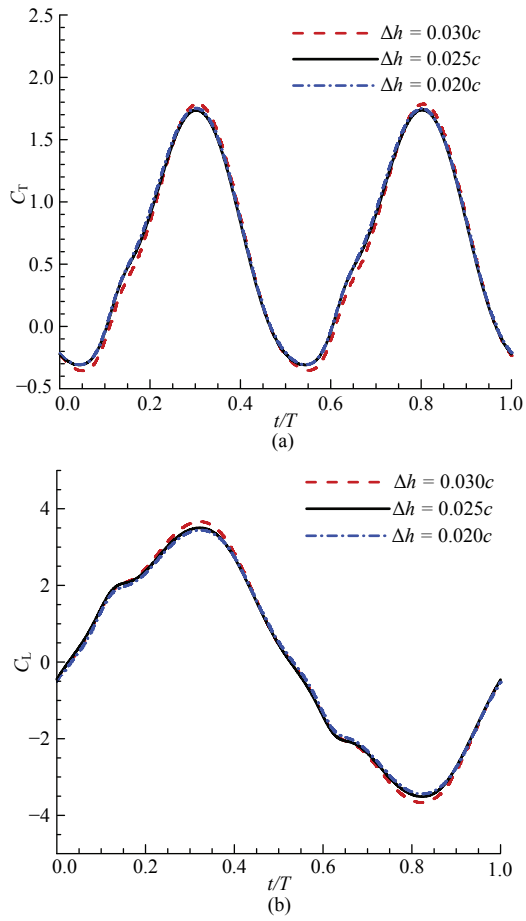

Fig. 3 Time histories of (a) thrust coefficient (C_T) and (b) lift coefficient obtained from different meshes.

the aerodynamics of a flapping foil[26–29]. The values of parameters used in current simulations are set as: $Re = 500$, $h_m/c = 1$, $\theta_m = \pi/6$, $f = 0.2$, $\theta_0 = 0$, $1.2 \le h_0/c \le 2.5$ and $0.25 \le S \le 0.75$. To make comparison, the cases of $h_0/c = \infty$, which represents no wall effect, are also simulated. In the first part, the wall effect of symmetric flapping foil ($S = 0.5$) will be studied, and then the asymmetric flapping foil will be investigated in the second part. Before that, the validation of mesh independence should be finished. To do that, the simulation at $S = 0.5$ and $h_0/c = \infty$ is performed. As shown in Fig. 3, the mesh spacing of $\Delta h = 0.025c$ is fine enough to achieve the accurate results.

3.1 Wall effect in symmetric motion

The force behaviours of the symmetric flapping foil near a wall, such as the mean thrust coefficient ($\overline{C}_T$) and the mean lift coefficient ($\overline{C}_L$), are shown in Fig. 4. The dash line represents the results of $h_0/c = \infty$. From the figure, it is found that the curves of $\overline{C}_T$ and $\overline{C}_L$ become steeper and steeper when the mean clearance (h_0) decreases. It indicates that the wall effect becomes stronger and stronger as the foil gradually approaches the wall. As shown in Fig. 4a, the presence of the wall can enhance $\overline{C}_T$ clearly. Meanwhile, the enhancement increases as h_0 decreases. However, $\overline{C}_L$ first increases and then decreased as h_0 decreases, as shown in Fig. 4b. The peak value of $\overline{C}_L$ occurs at $h_0/c = 1.5$. Moreover, one noted feature is that the negative $\overline{C}_L$ is produced if the foil is very close to the wall ($h_0/c < 1.3$). It implies that the decrease in h_0 is not always helpful for the lift generation. The negative wall effect, which restrains the lift generation, can be observed when the mean clearance is less than a threshold value.

To further check the variation of forces due to the wall effect, the time histories of thrust and lift coefficients (C_T and C_L) at $h_0/c = 1.2$, 1.5 and ∞ in one flapping

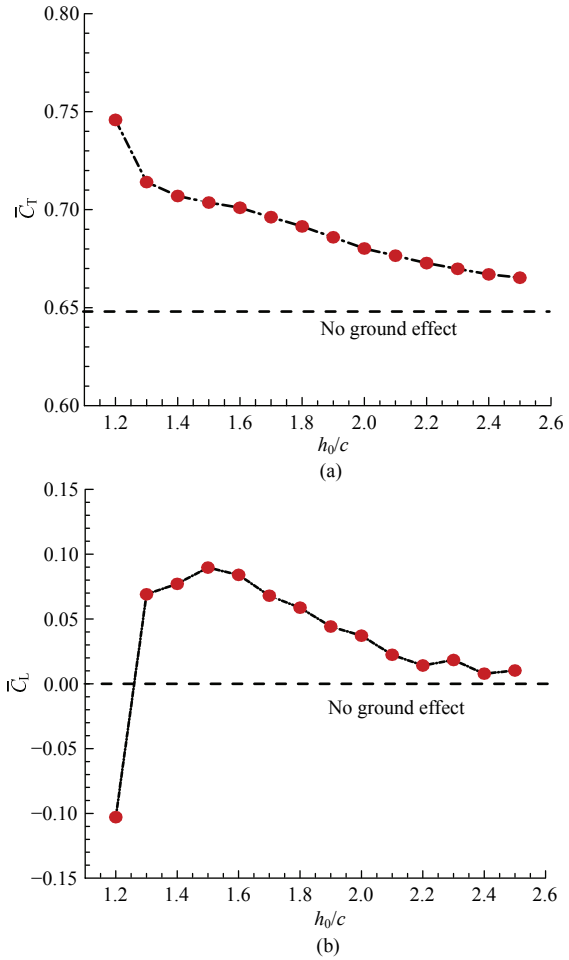

Fig. 4 (a) Mean thrust coefficient and (b) mean lift coefficient as function of mean clearance between foil and wall.

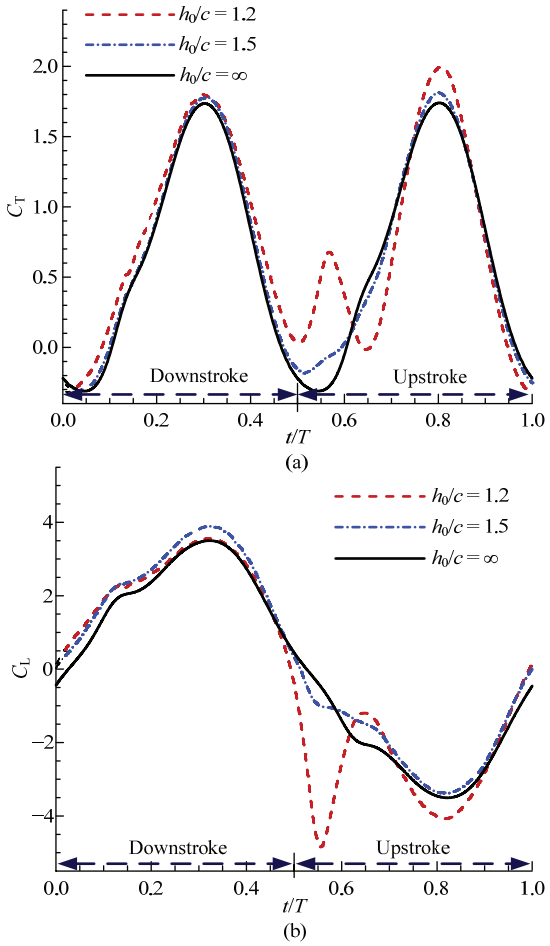

Fig. 5 Time histories of (a) thrust coefficient and (b) lift coefficient obtained from different clearances.

cycle are plotted in Fig. 5. As shown in Fig. 5a, two positive peaks of C_T can be observed at the instants of $t/T = 0.3$ and 0.8, respectively. For the case of $h_0/c = 1.2$, the peak value at $t/T = 0.8$ is higher than that of $h_0/c = \infty$. Moreover, it can be noted that C_T during the interval of t/T = 0.5–0.6 is strengthened significantly, and even a secondary peak is observed at about $t/T = 0.55$. For the case of $h_0/c = 1.5$, however, the wall effect is weakened, and the curve of C_T is close to that of $h_0/c = \infty$. As illustrated in Fig. 5b, on the other hand, C_L at $h_0/c = 1.2$ experiences a sharp decrease during the interval of $t/T = 0.5$–0.6 as compared with the case of $h_0/c = \infty$, and there is a negative peak value of C_L at $t/T = 0.55$. But when $h_0/c = 1.5$, C_L is increased more or less during the interval of $t/T = 0$–0.4.

Besides the force performance, the flow patterns can be also modified by the wall effect. Fig. 6 and Fig. 7, respectively, provide the instantaneous vorticity and pressure coefficient contours at two typical instants, *i.e.*, t/T = 0.55, 0.65 and 0.8. Again, the results at h_0/c = 1.2, 1.5 and ∞ are presented. Compared with the case of $h_0/c = \infty$ (Fig. 6c), strong interaction between the vortex shed from the foil and the wall happens for the case of h_0/c = 1.2 (Fig. 6a). As a result, the pressure distribution around the foil (Fig. 7a) differs from that at $h_0/c = \infty$ (Fig. 7c). For the case of h_0/c = 1.5 (Fig. 6b), however, the vortex interaction is greatly weakened. So the pressure distribution around the foil (Fig. 7b) is similar to that at $h_0/c = \infty$ (Fig. 7c).

In particular, at the earlier stage of upstroke (t/T = 0.55), the vortex is developing along the lower surface of the foil. As a result, the small distance between the foil and the wall induces an obvious low pressure region at the lower surface of the foil, as plotted in Fig. 7a. Consequently, both the increase in thrust and the decrease in lift occur, as shown in Figs. 5a and 5b,

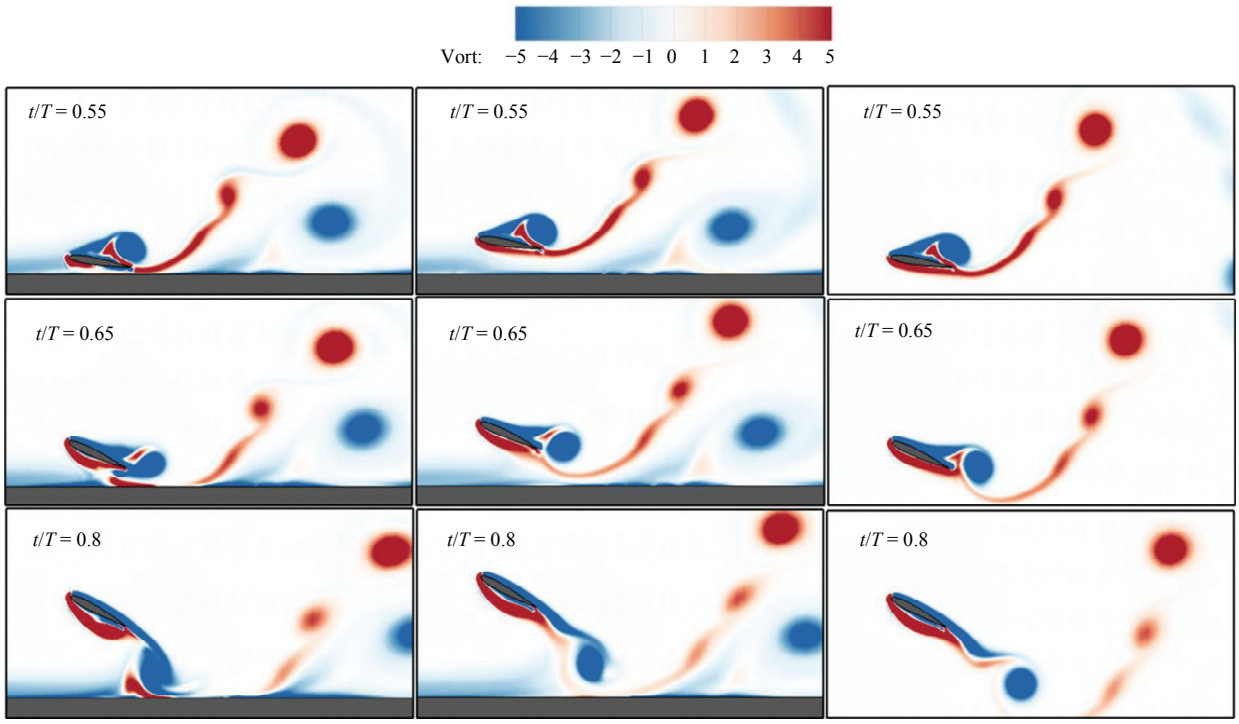

(a) $h_0/c = 1.2$ (b) $h_0/c = 1.5$ (c) $h_0/c = \infty$

Fig. 6 Instantaneous vorticity contours at different instants with different mean clearances.

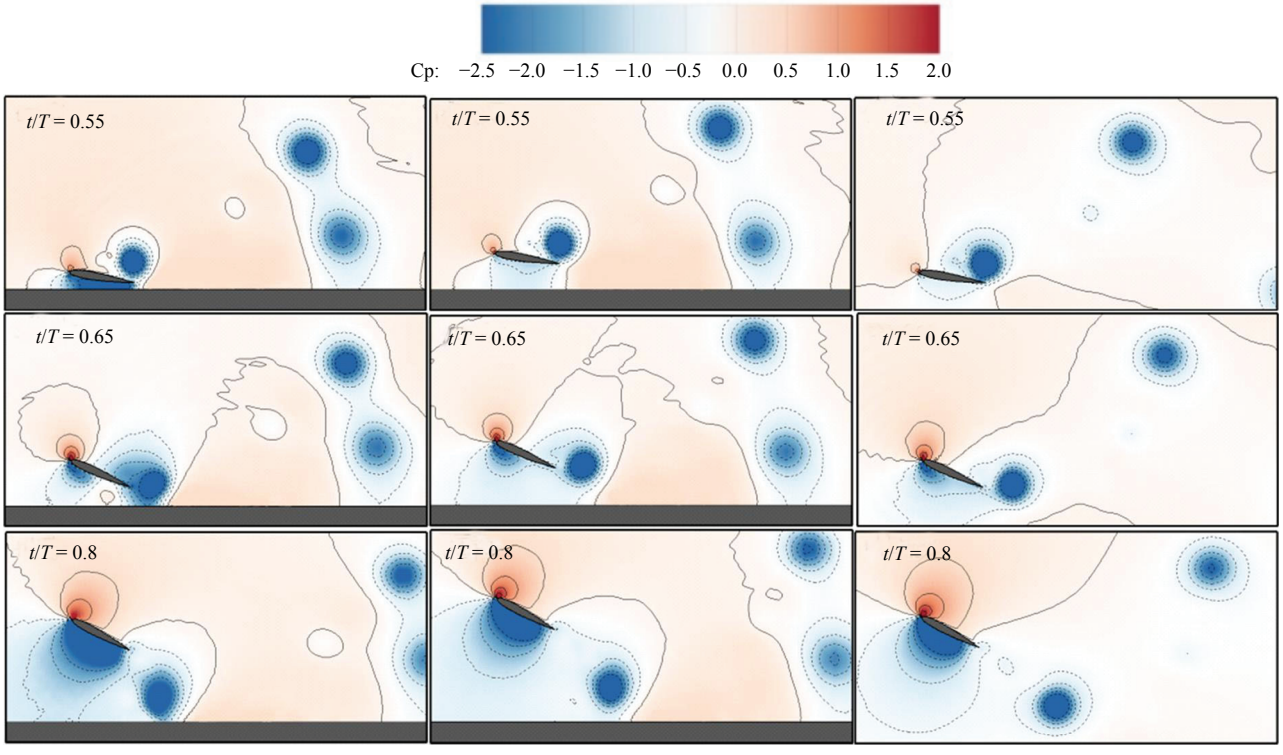

(a) $h_0/c = 1.2$ (b) $h_0/c = 1.5$ (c) $h_0/c = \infty$

Fig. 7 Instantaneous pressure coefficient contours at different instants with different mean clearances.

respectively. This is the reason why both the instantaneous thrust and lift coefficients have secondary peaks near the stroke reversal for the case of h_0/c = 1.2, as shown in Figs. 5a and 5b, respectively. When t/T = 0.65, the vortex is stagnated near the trailing edge of the foil, which results in the appearance of low pressure region at the upper surface of the foil. Consequently, small pressure difference between the lower and upper surfaces occurs as compared with the case of $h_0/c = \infty$. This is the reason why the thrust is decreased but the lift is increased at this instant as compared with the case of no wall effect, as shown in in Figs. 5a and 5b. When t/T = 0.8, a new Leading Edge Vortex (LEV) is forming along the lower surface of the foil, which results in the low pressure region on the lower surface. Comparing the results in Figs. 7a and 7c at this instant, it is found that the low pressure region on the lower surface is elongated by the wall significantly. This phenomenon causes the thrust enhancement and lift reduction as shown in Figs. 5a and 5b. Therefore, flapping much close to the wall may be harmful due to the negative lift.

Based on the results above, it is known that to generate both high mean thrust and positive mean lift in wall effect, the mean clearance between foil and wall should be larger than a critical value. Moreover, the wall effect mainly changes the force behavior during the upstroke of flapping foil. Thus, in order to further enhance the mean thrust or mean lift, the duration of upstroke can be modified. In the following section, the asymmetric heaving motion then will be introduced into the wall effect.

3.2 Wall effect in asymmetric motion

The asymmetric heaving motion is controlled by the coefficient S, as defined in Eq. (2). When $S < 0.5$, the downstroke duration is less than the upstroke one, and vice versa. Fig. 8 plots the variation of $\bar{C}_T$ and $\bar{C}_L$ with respect to S at h_0/c = 1.2, 1.5, 2 and ∞.

From Fig. 8a, it is indicated that $\bar{C}_T$ first decreases and then increases with the increase in S for the cases of h_0/c = 1.5, 2 and ∞. In addition, the results at h_0/c = 2 is approximate to that at $h_0/c = \infty$, which means that the wall effect has been weakened obviously. As the foil is very close to the wall, *i.e.*, h_0/c = 1.2, the variation of $\bar{C}_T$ is complex when $S > 0.5$. It vibrates around the value of $\bar{C}_T \approx 0.7$. On the other hand, by changing h_0, $\bar{C}_T$ can demonstrate different variation trend at a fixed S. Without considering the case of h_0/c = 1.2, there are two typical regimes, *i.e.*, monotonic reduction and monotonic enhancement. When $S < 0.4$, $\bar{C}_T$ experiences a monotonic reduction as h_0 decreases. It means that the wall effect is harmful for the thrust generation. The similar negative wall effect has also been observed in the previous work[18,19]. When $S > 0.4$, $\bar{C}_T$ increases monotonically as h_0 decreases. Thus, the wall effect under this condition is beneficial for the thrust generation, which is similar to the positive wall effect that reported in many previous studies[15–17].

From Fig. 8b, it is found that $\bar{C}_L$ always can decrease with S monotonically for all values of h_0 considered. In particular, $\bar{C}_L$ is positive when $S < 0.5$ and negative when $S > 0.5$. It implies that the short downstroke duration is beneficial for the lift generation. Moreover, for a given S, the value of $\bar{C}_L$ at different h_0 is close to each other when $S < 0.5$. It then means that the influence of wall effect on $\bar{C}_L$ is weaker than that of the asymmetric heaving motion when $S < 0.5$. From the results in Fig. 8, it is known that the wall effect in the asymmetric flapping motion becomes complex. To enhance the mean thrust, the upstroke duration should be shortened. But to generate the positive mean lift, the downstroke duration needs to be reduced.

Similar to Fig. 5, Fig. 9 illustrates the time histories of C_T and C_L in one flapping cycle. Since the curves change sharply for the case of h_0/c = 1.2, only the results at h_0/c = 1.5 are presented. Two asymmetric coefficients, *i.e.*, S = 0.3 and 0.7 are selected. Moreover, the results at S = 0.5 are also involved for comparison.

From Fig. 9a, compared with the case of S = 0.5, although C_T at S = 0.3 is enlarged clearly during the most part of downstroke, it is reduced significantly during the whole upstroke. Since the upstroke duration is longer, the resultant $\bar{C}_T$ then is still reduced. The opposite situation can be observed for the case of S = 0.7. Here, the difference of mean thrust coefficient can be defined as $\Delta\bar{C}_T = \bar{C}_{T,S=i} - \bar{C}_{T,S=0.5}$, where i = 0.3, 0.7, the positive and negative differences are identified as $\Delta\bar{C}_T^+$ and $\Delta\bar{C}_T^-$, respectively. For the case of S = 0.3, $\Delta\bar{C}_T^+$ = 0.57 and $\Delta\bar{C}_T^-$ = −0.76. As a consequence, $\Delta\bar{C}_T$ = −0.19, namely, the thrust is decreased. As for case of S = 0.7, $\Delta\bar{C}_T^+$ = 0.91 and $\Delta\bar{C}_T^-$ = −0.65. As a result, $\Delta\bar{C}_T$ = 0.26, namely, the thrust is increased. From Fig. 9b, the peak value of C_L at S = 0.3 during the downstroke is increased

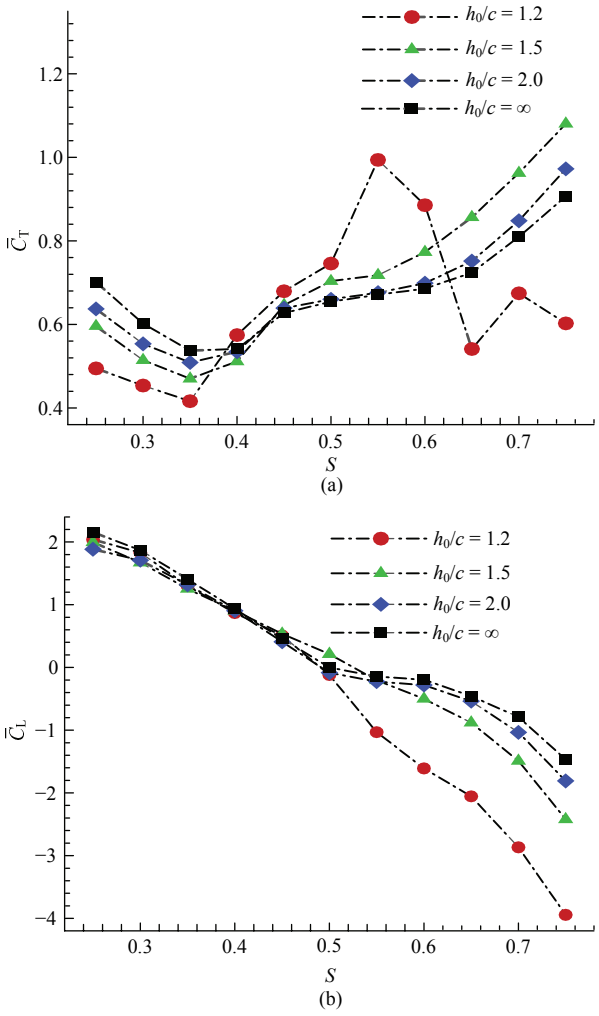

Fig. 8 (a) Mean thrust coefficient and (b) mean lift coefficient varying with asymmetric coefficient.

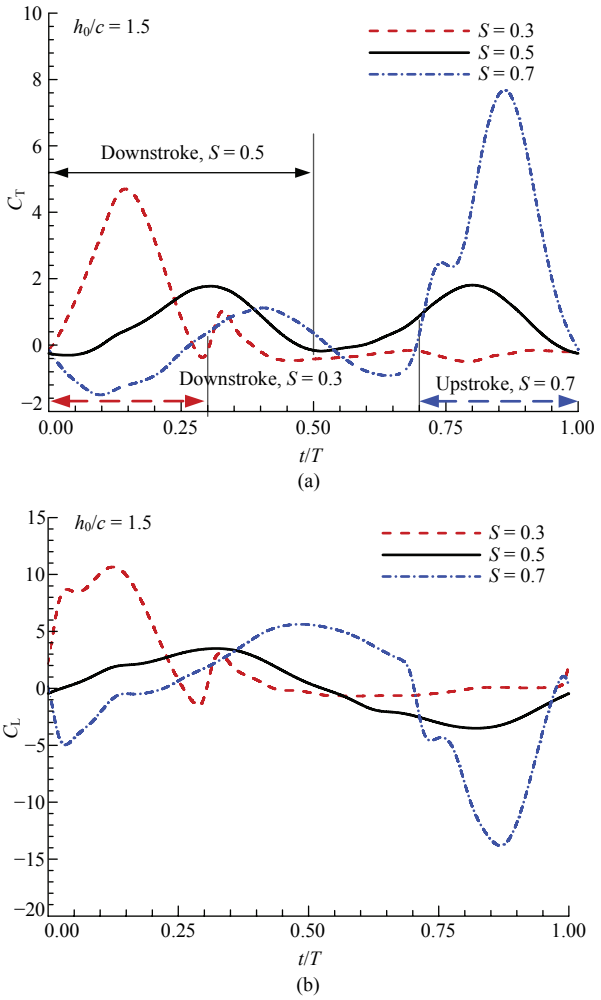

Fig. 9 Time histories of (a) thrust coefficient and (b) lift coefficient at different asymmetric coefficients.

obviously as compared with the case of $S = 0.5$. In the meanwhile, C_L during the upstroke is nearly close to be zero. As a sequence, the generated $\bar{C}_L$ is positive. Again, the opposite situation happens for the case of $S = 0.7$.

Similar to Fig. 6 and Fig. 7, the instantaneous vorticity and pressure coefficient contours ($h_0/c = 1.5$, $S = 0.3$, 0.5 and 0.7) at four typical instants are presented in Fig. 10 and Fig. 11, respectively. It should be noted that the contours ranges in these two figures are the same as that in Fig. 6 and Fig. 7.

At the instant of $t/T = 0.2$, the foil is moving downward. For the case of $S = 0.3$, a clear leading edge vortex has been formed. It is developing along the upper surface of the foil due to the dynamic stall, as shown in Fig. 10a. As compared with the case of $S = 0.5$, as shown in Fig. 10b, the size of LEV is larger. In addition, the foil is also plunging faster. Therefore, as shown in Fig. 11a, a lower pressure region is produced along the upper surface and a higher one along the lower surface. For the case of $S = 0.7$ shown in Fig. 10c, however, no clear LEV can be found. So the pressure along the lower surface is lower than that along the upper surface, as shown in Fig. 11c.

At the instant of $t/T = 0.5$, the foil with $S = 0.5$ just reaches its lowest position of heaving motion. The LEV is leaving the upper surface. Nevertheless, the foil with $S = 0.3$ has already come to the upstroke. The LEV has been shed into the wake, and a new LEV is being generated along the lower surface. So a high pressure region is formed around the leading edge of upper surface. In contrast, the foil with $S = 0.7$ is still carrying out its downstroke and approaching the wall. At this moment, the pressure along the lower surface is higher than that along the upper surface.

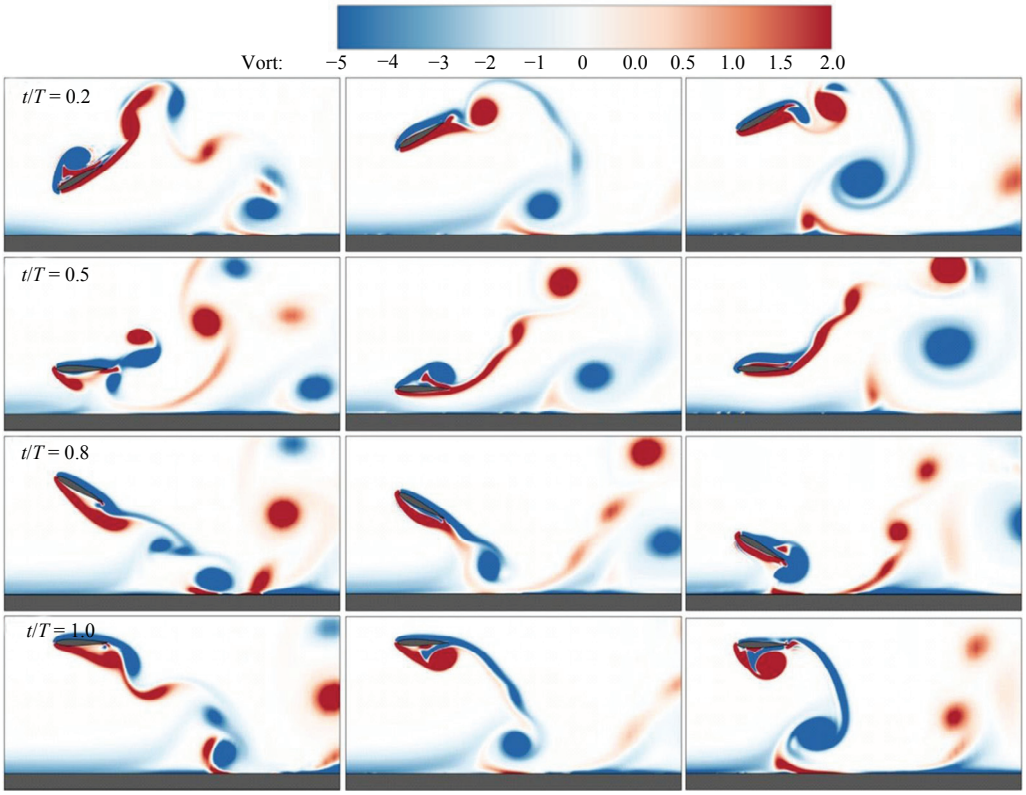

Fig. 10 Instantaneous vorticity contours at different instants and asymmetric coefficients with h_0/c = 1.5.

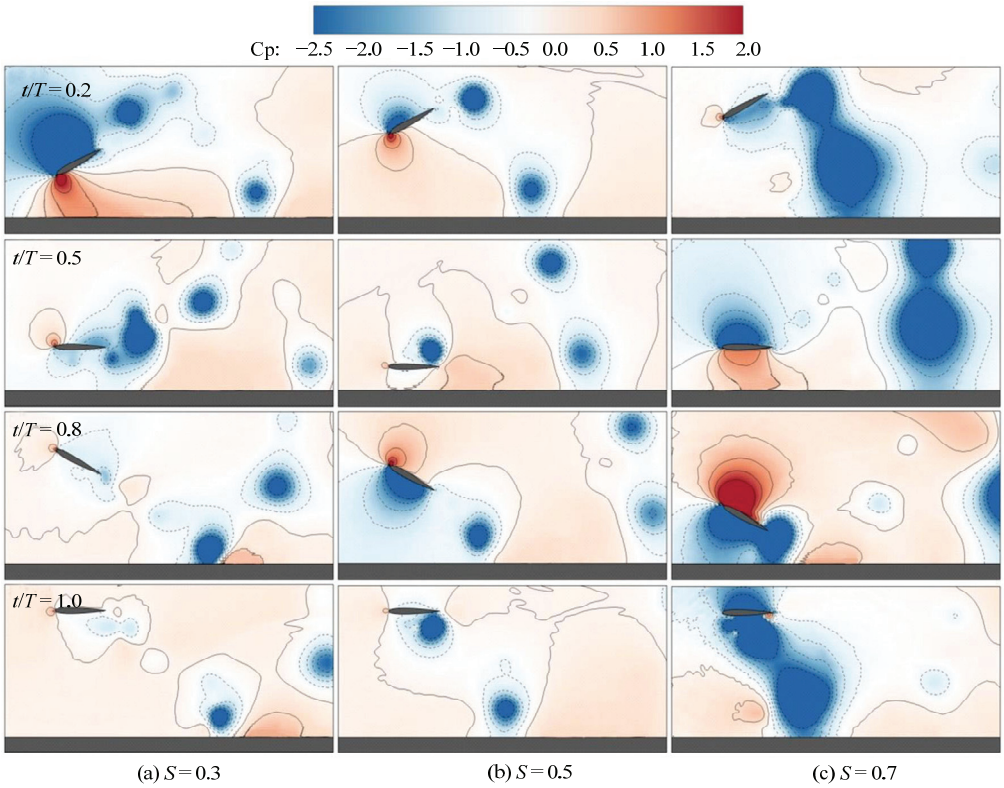

Fig. 11 Instantaneous pressure coefficient contours at different instants and asymmetric coefficients with h_0/c = 1.5.

At the instant $t/T = 0.8$, the foil is moving upward. For the case of $S = 0.3$, the heaving velocity of the foil is slower than that of $S = 0.5$. The newly formed LEV is greatly elongated along the lower surface. As a result, no clear pressure difference between the upper surface and lower surface is observed. For the case of $S = 0.7$, the foil is speeding up, and a new LEV starts to be produced along the lower surface. Consequently, great pressure difference between the upper surface and lower surface appears.

At the instant $t/T = 1.0$, the foil just finishes a complete cycle of flapping motion. When $S = 0.3$, the LEV is only shed partly. So there is no clear pressure difference between two surfaces yet. When $S = 0.7$, on the contrary, the new LEV is very strong and developing along the lower surface. However, the pressure along the upper surface is also low, which then reduces the pressure difference between two surfaces. The flow patterns in Fig. 10 and Fig. 11 explain well the force behavior in Fig. 9.

4 Conclusion

In this work, the aerodynamic performance of a two-dimensional flapping foil with asymmetric heaving motion in wall effect is investigated. To perform the numerical simulation, an immersed boundary-simplified circular function-based gas kinetic scheme is adopted. The effects of the clearance between foil and wall and the asymmetric coefficients are investigated systematically. Based on the numerical results, it is found that the force behavior is affected by both the wall effect and asymmetric heaving motion significantly. When only the wall effect is considered, the mean thrust monotonically increases as the foil approaches the wall gradually. At the same time, the mean lift first increases and then decreases suddenly. If the foil is very close to the wall, the mean lift even becomes negative. When the asymmetric heaving motion is also involved, the variation of forces becomes complex. When the duration of upstroke is decreased, the foil experiences the enhancement of mean thrust. In addition, further enhancement can be obtained when the clearance between foil and wall decreases. When the downstroke duration is shorter than the upstroke duration, the positive mean lift can be observed. After checking the flow patterns around the foil, it is demonstrated that the interaction between the vortex shed from the foil and the wall greatly changes the pressure distribution along the foil surface. In summary, a flapping foil heaving quickly during the downstroke but slowly during the upstroke is an effective strategy when it is advance near a wall. The results in this work may be used to optimize the kinematics of the MAVs flying near a wall or water surface. On the other hand, it is noted that the flexible deformation also affects the aerodynamic performance of a flapping foil, and it will be our future work.

Acknowledgment

This work is supported by Fundamental Research Funds for the Central Universities (Grant No. NE2017102), Priority Academic Program Development of Jiangsu Higher Education Institutions (PAPD).

References

[1] Quinn D B, Moored K W, Dewey P A, Smits A J. Unsteady propulsion near a solid boundary. *Journal of Fluid Mechanics*, 2014, **742**, 152–170.

[2] Cui E, Zhang X. Wall effect aerodynamics. *Encyclopedia of Aerospace Engineering*, 2010, **59**, 245–256.

[3] Blake R W. Mechanics of gliding in birds with special reference to the influence of the wall effect. *Journal of Biomechanics*, 1983, **16**, 649–654.

[4] Withers P C, Timko P L. The significance of wall effect to the aerodynamic cost of flight and energetics of the black skimmer (*Rhyncops Nigra*). *Journal of Experimental Biology*, 1977, **70**, 13–26.

[5] Hainsworth F R. Induced drag savings from wall effect and formation flight in brown pelicans. *Journal of Experimental Biology*, 1988, **135**, 431–444.

[6] Webb P W. The effect of solid and porous channel walls on steady swimming of steelhead trout oncorhynchus mykiss. *Journal of Experimental Biology*, 1993, **178**, 97–108.

[7] Kim E J, Wolf M, Ortega-Jimenez V M, Cheng S H, Dudley R. Hovering performance of Anna's hummingbirds (*Calypte anna*) in wall effect. *Journal of the Royal Society Interface*, 2014, **11**, 20140505.

[8] Park H, Choi H. Aerodynamic characteristics of flying fish in gliding flight. *Journal of Experimental Biology*, 2010, **213**, 3269–3279.

[9] Wiesesberger C. Wing resistance near the wall. *Zeitschrift fur Flugtechnik Motorluftschiffahrt*, 1921, **10**, 145–147.

[10] Quinn D B, Lauder G V, Smits A J. Flexible propulsors in

wall effect. *Bioinspiration & Biomimetics*, 2014, **9**, 036008.

[11] Moryossef Y, Levy Y. Effect of oscillations on airfoils in close proximity to the wall. *AIAA Journal*, 2004, **42**, 1755–1764.

[12] Birch J M, Dickson W B, Dickinson M H. Force production and flow structure of the leading edge vortex on flapping wings at high and low Reynolds numbers. *Journal of Experimental Biology*, 2004, **207**, 1063–1072.

[13] Rayner J M V. On the aerodynamics of animal flight in wall effect. *Philosophical Transactions of the Royal Society B*: *Biological Sciences*, 1991, **334**, 119–128.

[14] Srinidhi N G, Vengadesan S. Wall effect on tandem flapping wings hovering. *Computers & Fluids*, 2017, **152**, 40–56.

[15] Dai L, He G, Zhang X. Self-propelled swimming of a flexible plunging foil near a solid wall. *Bioinspiration & Biomimetics*, 2016, **11**, 046005.

[16] Fernández-Prats R, Raspa V, Thiria B, Huera-Huarte F, Godoy-Diana R. Large-amplitude undulatory swimming near a wall. *Bioinspiration & Biomimetics*, 2015, **10**, 016003.

[17] Gao T, Lu X Y. Insect normal hovering flight in wall effect. *Physics of Fluids*, 2008, **20**, 087101.

[18] Kolomenskiy D, Maeda M, Engels T, Liu H, Schneider K, Nave J C. Aerodynamic wall effect in fruitfly sized insect takeoff. *PLOS ONE*, 2016, **11**, e0152072.

[19] Wu J, Shu C, Zhao N, Yan W. Fluid dynamics of flapping insect wing in wall effect. *Journal of Bionic Engineering*, 2014, **11**, 52–60.

[20] Truong T V, Byun D, Kim M J, Yoon K J, Park H C. Aerodynamic forces and flow structures of the leading edge vortex on a flapping wing considering wall effect. *Bioinspiration & Biomimetics*, 2013, **8**, 036007.

[21] Truong T V, Kim J, Kim M J, Park H C, Yoon K J, Byun D. Flow structures around a flapping wing considering wall effect. *Experiments in Fluids*, 2013, **54**, 1575.

[22] Sarkar S, Venkatraman K. Numerical simulation of incompressible viscous flow past a heaving airfoil. International *Journal for Numerical Methods in Fluids*, 2006, **51**, 1–29.

[23] Yang L M, Shu C, Yang W M, Wang Y, Wu J. An immersed boundary-simplified sphere function-based gas kinetic scheme for simulation of 3D incompressible flows. *Physics of Fluids*, 2017, **29**, 083605.

[24] Yang L M, Shu C, Wu J, Zhao N, Lu Z L. Circular function-based gas-kinetic scheme for simulation of inviscid compressible flows. *Journal of Computational Physics*, 2013, **255**, 540–557.

[25] Wu J, Shu C. Implicit velocity correction-based immersed boundary-lattice Boltzmann method and its applications. *Journal of Computational Physics*, 2009, **228**, 1963–1979.

[26] Guerrero J E. Effect of cambering on the aerodynamic performance of heaving airfoils. *Journal of Bionic Engineering*, 2009, **6**, 398–407.

[27] Le T Q, Byun D, Park S H, Ko J H, Park H C. Effect of chord flexure on aerodynamic performance of a flapping wing. *Journal of Bionic Engineering*, 2010, **7**, 87–94.

[28] Shyy W, Liang Y, Tang J, Liu H, Trizila O, Stanford B, Bernal L, Cesnik C, Friedmann P, Ifju P. Computational aerodynamics of low Reynolds number plunging, pitching and flexible wings for MAV applications. *Acta Mehcanica Sinica*, 2008, **24**, 351–374.

[29] Aono H, Liu H. Near- and far-field aerodynamics in insect hovering flight: An integrated computational study. *Journal of Experimental Biology*, 2008, **211**, 239–257.